Quantum resonance in an intrinsically degenerate system: Nonlinear cyclotron resonance

V. Ya. Demikhovskii and D. I. Kamenev
Nizhny Novgorod State University, Nizhny Novogorod 603600, Russia

G. A. Luna-Acosta*
Ilya Prigogine Center for Statistical Mechanics and Complex Systems, The University of Texas at Austin, Austin, Texas 78712
(Received 28 October 1994; revised manuscript received 8 May 1995)

The quantum dynamics of a charged particle gyrating in a uniform magnetic field and interacting with a monochromatic wave is investigated here under the condition of cyclotron resonance. The classical counterpart of this system is intrinsically degenerate. The structure of the Floquet spectrum and quasienergy functions for the exact and near resonance cases is obtained and related to the classical phase space structure. The evolution of various representative initial states is investigated and the close connection between classical and quantum dynamics at nonlinear cyclotron resonance is demonstrated. The condition for the experimental realization of the acoustic quantum nonlinear cyclotron resonance in conductors is given, and the influence of sound waves on some oscillatory phenomena in quantizing magnetic fields is predicted.

PACS number(s): 05.45.+b, 03.65.Sq, 03.65.Bz

In recent years the phenomenon of nonlinear quantum resonance in two-dimensional systems and one-dimensional systems driven by a periodic external field has been investigated in detail [1–5]. The properties of their spectra and eigenfunctions were explored. Among other things, it was shown that, analogous to the classical case, quantum nonlinear resonances for a small perturbation parameter remain isolated in Hilbert space. However, as this parameter is increased resonances can overlap, leading to an extension of the wave function. To our knowledge, nonlinear quantum resonance has been studied only in systems whose classical counterpart is accidentally degenerate and the conditions of the Kolmogorov, Arnold, Moser theorem are satisfied. In this work we will treat the quantum resonance in a system whose classical analog is intrinsically degenerate. An important and simple physical model of such a system is a particle moving in a constant magnetic field **H** perturbed by a monochromatic wave spreading perpendicularly to the vector **H**. In solid state physics this system can be realized in metals, semiconductors, and low-dimensional semiconductor structures.

Classical nonlinear cyclotron resonance has been studied extensively in plasma physics [6–8] and in solid state physics [9]. Chernikov and collaborators [10] have shown that for the exact resonance case, the dynamics of a simple harmonic oscillator (SHO) perturbed by a wave field is much richer than that of a nonlinear SHO that is equally perturbed. This is so mainly because no KAM tori exists to limit diffusion. The phase space portrait in action-angle variables of the perturbed SHO consists of a separatrix lattice enclosing elliptic orbits and forming rectangular cells. Two such cells are shown in Fig. 1(a). This interesting feature of a classical intrinsically degenerate system makes its quantum counterpart a very attractive subject for investigation. Some interesting quantum aspects (e.g., the time of classical description and diffusion) of the periodically kicked SHO have been investigated in [11].

We first give here a brief review of some essential aspects of the classical problem (for details, see Ref. [8]). The Hamiltonian of the charged particle moving in both magnetic and monochromatic wave fields has the form

$$H=\frac{\left[\mathbf{p}-\frac{e}{c}\mathbf{A}\right]^2}{2m}-V_0\cos(kx-\omega t)\ , \tag{1}$$

where the gauge $\mathbf{A}\ (0,Hx,0)$ was chosen to produce a magnetic field along the z direction, m is the mass of the particle, $\mathbf{p}$ is the momentum, $\mathbf{k}$ is the wave vector, ω is the wave frequency, and V_0 is the amplitude of perturbation.

The first order perturbation theory near a resonance gives the following Hamiltonian [8]:

$$\tilde{H}=\tilde{I}\delta\omega-J_l(kr(\tilde{I}))\cos\tilde{\theta}\ , \tag{2}$$

where $\tilde{I}$ and $\tilde{\theta}$ are the resonant canonical conjugate action-angle variables, $\delta\omega=l\omega_c-\omega$, l is the number of resonance, $l=1,2,\ldots$, $\omega_c=eH/mc$ is the cyclotron frequency, and $J_l(kr)$ is the Bessel function of order l. When $\delta\omega=0$ the elliptic fixed points are determined by

$$\frac{dJ_l(kr(\tilde{I}))}{d\tilde{I}}=0,\quad \tilde{\theta}=0,\pi\ , \tag{3}$$

and the hyperbolic points by

*On sabbatical leave from Instituto de Fisica, Universidad Autonoma de Puebla, Apartado Postal J-48, 72570 Puebla, Puebla, Mexico.

$$J_l(kr(\tilde{I}))=0, \quad \tilde{\theta}=\pi/2, \quad \tilde{\theta}=3\pi/2 \ . \tag{4}$$

The size of a lattice cell in action is limited by two neighboring roots of the Bessel function of order l; see Fig. 1(a). It is important to note that the size of the cells is independent of the amplitude of perturbation V_0.

In this first order approximation, the system described by (2) is integrable, unlike the exact system described by the Hamiltonian (1). If nonresonant terms are taken into account in (1), then the separatrices become a stochastic web whose thickness decays exponentially with the distance from the initial cell [10]. Traveling along the web, particles diffuse to greater energies.

The quantum version of our system is described by the Hamiltonian

$$\hat{H}=\hat{H}_0-V_0\cos(kx-\omega t) \ , \tag{5}$$

where $\hat{H}_0$ is the SHO Hamiltonian

$$\hat{H}_0=\frac{\hat{p}_x^2}{2m}+\frac{m\omega_c^2}{2}(x-x_0)^2+\frac{\hat{p}_z^2}{2m} \ . \tag{6}$$

The momenta p_z and p_y are integrals of the motion, so the last term in $\hat{H}_0$ can be omitted. The center of the oscillations, $x_0=cp_y/eH$, is constant and one can exclude it in (6) by choosing the initial time $t=t_0$ appropriately. Henceforth we set $t_0=0$ and our problem is then equivalent to that of a one-dimensional quantum SHO driven by a monochromatic wave.

It is convenient to choose SHO bases to expand the state vector,

$$\psi(x,t)=\sum_n C_n(t)\psi_n(x)\exp(-iE_nt/\hbar) \ , \tag{7}$$

where $\psi_n(x)$ is the nth eigenfunction of the SHO Hamiltonian $\hat{H}_0$ and $E_n=\hbar\omega_c(n+\frac{1}{2})$ is the energy on the nth Landau level. Using (7), the nonstationary Schrödinger equation

$$i\hbar\frac{\partial\psi(x,t)}{\partial t}=\hat{H}\psi(x,t) \tag{8}$$

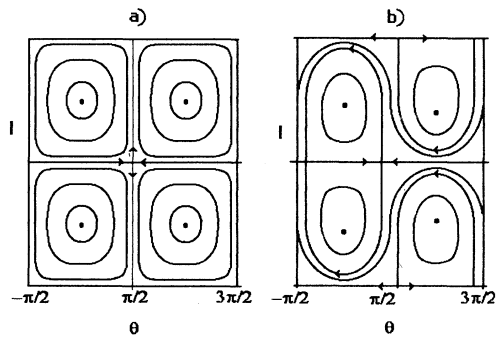

FIG. 1. Phase portrait in action-angle variables of the system described by Hamiltonian (2). The horizontal parts of the separatrix correspond to action values such that $J_l(kr(I))=0$. (a) The exact resonance case $\delta\omega=0$. (b) The near resonance case $\delta\omega\neq0$.

becomes

$$i\hbar\dot{C}_n=\sum_m [V^{(1)}_{n,n+m}\sin(\omega t)+V^{(2)}_{n,n+m}\cos(\omega t)] \times C_{n+m}e^{-im\omega_c t} \ . \tag{9}$$

The matrix elements $V^{(1)}_{n,n+m}$ ($V^{(2)}_{n,n+m}$) describe the transitions between levels of opposite (equal) parity. They are expressed via the Laguerre polynomials as [12]

$$V^{(1)}_{n,n+2m+1}=-V_0\frac{(-1)^m\mu^{2m}e^{-\mu^2/4}}{2^{m+1}\sqrt{(n+1)\cdots(n+2m+1)}} \times L_n^{2m+1}\left[\frac{\mu^2}{2}\right] , \tag{10a}$$

$$V^{(2)}_{n,n+2m}=-V_0\frac{(-1)^m\mu^{2m}e^{-\mu^2/4}}{2^{m+1}\sqrt{(n+1)\cdots(n+2m)}}L_n^{2m}\left[\frac{\mu^2}{2}\right] , \tag{10b}$$

where $\mu=ka$, $a=\sqrt{\hbar c/eH}$ is the magnetic length, and L_n^{2m} are the Laguerre polynomials. When $n\gg1\gg\mu^2/2$, the Laguerre polynomials can be expressed in terms of the Bessel functions [12],

$$L_n^{2m}\left[\frac{\mu^2}{2}\right]=\left[\frac{2n}{\mu^2}\right]^m J_{2m}(kr_n) \ , \tag{11}$$

where $r_n=\sqrt{2na}$. For calculation purposes we confine ourselves to the case $n\gg1\gg\mu^2/2$ and obtain the following expression for the matrix elements:

$$V^{(1)}_{n,n+2m+1}=-\frac{V_0}{2}\frac{(-1)^m n^{m+1/2}e^{-\mu^2/4}}{\sqrt{(n+1)\cdots(n+2m+1)}} \times J_{2m+1}(kr_n) \ , \tag{12a}$$

$$V^{(2)}_{n,n+2m}=-\frac{V_0}{2}\frac{(-1)^m n^m e^{-\mu^2/4}}{\sqrt{(n+1)\cdots(n+2m)}}J_{2m}(kr_n) \ . \tag{12b}$$

All terms in the sum in (9) are of the same order in the amplitude V_0, but they differ in their frequency of oscillation. Keeping only the resonant terms in (9) we obtain

$$i\hbar\dot{C}_n=V^{(j)}_{n,n+l}C_{n+l}+V^{(j)}_{n,n-l}C_{n-l} \ , \tag{13}$$

where $j=1$ (2) for odd (even) resonance number l. Incidentally, if we were to consider effects such as second order resonances, their overlapping, and their relation to quantum chaos, we would have needed to include nonresonant terms in (9).

Since the perturbation is periodic in time, Floquet theory can be used to determine the time evolution of the system in terms of quasienergy (QE) spectra E_q and QE functions $\Psi_q(x,t)$. Then the QE eigenfunctions of the evolution operator for one period of oscillation of the external field, $T=2\pi/\omega$, can be written as

$$\Psi_q(x,t)=\exp\left[-\frac{iE_qt}{\hbar}\right]U_q(x,t) \ , \tag{14}$$

where $U_q(x,t)=U_q(x,t+T)$. As in Eq. (7) we expand $U_q(x,t)$ on a SHO basis,

$$U_q(x,t)=\sum_n C_n^q(t)\psi_n(x) . \tag{15}$$

Coefficients $C_n^q(t)$ are periodic functions of t and can be expanded in a Fourier series

$$C_n^q(t)=\sum_s A_{n,s}^q \exp(-is\omega t) . \tag{16}$$

After substituting Eqs. (14), (15), and (16) into the Schrödinger Eq. (8), we obtain the following system of uniform algebraic equations:

$$(E_q-\hbar\omega_c n+\hbar\omega s)A_{n,s}^q=\sum_m V_{n,m}^{(j)}(A_{m,s+1}^q+A_{n,s-1}^q) \tag{17}$$

(see, for example, Ref. [13], formula 9.2.18, p. 386), where the quasienergy E_q is measured from the ground state $\hbar\omega_c/2$. We can solve Eq. (17) for two distinct cases; namely, the resonant and near resonant cases. We calculate E_q and $A_{n,s}^q$ by perturbation theory assuming $V_0/\hbar\omega \ll 1$. Furthermore, for the near resonant case $(\omega_c-\omega=\delta\omega)$ we also assume that E_q is proportional to V_0 and that $\hbar\delta\omega n \ll \hbar\omega$ for all values of n considered here. Under these conditions we have, to zeroth order approximation,

$$(\hbar\omega s-\hbar\omega_c n)A_{n,s}^q=0 .$$

Hence,

$$A_{n,s}^q=0 \quad \text{for } n\neq s, \quad A_{n,s}^q\equiv A_n^q \quad \text{for } n=s .$$

To first order approximation, Eq. (17) yields

$$(E_q-\hbar\delta\omega n)A_n^q=V_{n,n+1}^{(1)}A_{n+1}^q+V_{n,n-1}^{(1)}A_{n-1}^q . \tag{18}$$

In a similar manner one can deduce for any resonant number l its corresponding QE-eigenvalue equation. The QE spectrum E_q and its eigenvectors A_n^q, where n is the nth component of qth QE vector, can be obtained by numerical diagonalization. Figures 2 and 3 illustrate the results of our calculation for the case of exact resonance. The matrix elements $V_{n,n+1}^{(1)}$, which are proportional to the Bessel function [see (12)a], are shown on the top of Fig. 2 as a function of n. The argument of the Bessel function is $kr_n=\sqrt{2nh}$, where $h=k^2a^2=k^2c\hbar/eH$. Thus h is the effective Planck's constant for our problem. We see that the plot of these matrix elements as a function of n define "quantum resonance cells" in Hilbert space delimited by the zeros of the Bessel function. That is, if the initial state is located in a certain cell, then almost all subsequent dynamics described by Eq. (13) will occur in this individual cell because the matrix elements are small on the boundaries of the cell and hence the transition probabilities here are small, too. This can be shown also from Eq. (18), where the off-diagonal modulation causes the system to break into a series of the weakly interacting parts. Figure 2 shows three such cells and four spectra. Note here that all E_q are proportional to

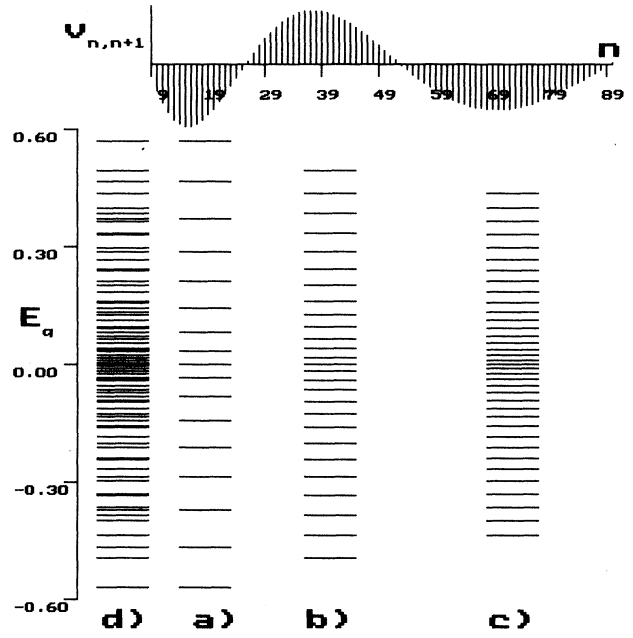

FIG. 2. Matrix elements and QE spectrum for the exact resonance case. The energy scale is in arbitrary units, $V_0=2.0$, and the effective Planck constant $h=1$.

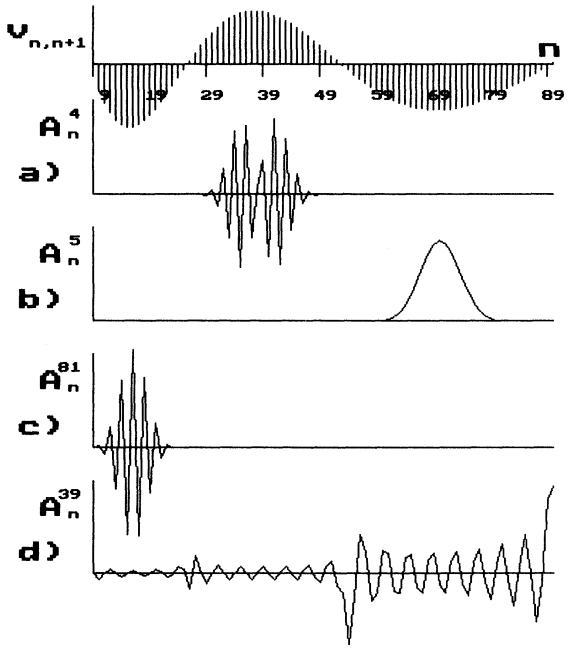

FIG. 3. QE functions A_n^q as a function of n for the exact resonance case. (a) $q=4$, (b) $q=5$, (c) $q=81$, (d) $q=39$. q labels the qth QE state in ascending order from the bottom of the spectrum. The values of V_0 and h are the same as in Fig. 2.

V_0 [cf. Eqs. (18) and (12)]; therefore the results of our calculations presented in Fig. 2 can be used to obtain QE spectra for an arbitrary V_0. Each spectrum, (a)–(c), corresponds to the solution of Eq. (18) considering only those unperturbed states that lie in their respective cells. Spectrum (d) is calculated including the total number of states in all three cells. An inspection of Fig. 2 shows that the range of each individual spectrum is roughly proportional to the maximum of the matrix element of its corresponding cell, $\pm|V^{\max}_{n,n+l}|$. We wish to remark that these energy intervals correspond to the intervals where the classical Hamiltonian (2) changes from $-V_0J_l(kr)$ to $+VJ_l(kr)$ as $\cos\theta$ varies from -1 to $+1$. Moreover, we see from Fig. 1(a) that this energy interval encloses two classical resonant cells. Thus, one Hilbert cell corresponds to two classical cells. Note also that all spectra are symmetrical and the number of QE states of each individual cell is equal to the number of unperturbed eigenstates in its corresponding cell. These features are due to the structure and size, respectively, of the determinant of the system (18). Furthermore the spectrum is very nearly equidistant near the top and bottom of the energy interval corresponding to each individual cell. Analytically, we can show this feature by expanding the matrix elements in the neighborhood of its maximum absolute value, $n=n_0$, and expressing A^q_n (as in [14] p. 259) in the form

$$A^q_n=\frac{1}{2\pi}\int_0^{2\pi}d\phi a(\phi)\exp[i(n-n_0)\phi]\ . \tag{19}$$

This procedure yields two Schrödinger equations differing only by the sign of their potential, which is that of a SHO. They give the equidistant separation of QE levels that we observe at the top and the bottom of the spectrum [see Figs. 2(a)–2(c)]. The frequency $\tilde{\omega}$ of this oscillator gives the following distance between QE levels:

$$\hbar\tilde{\omega}=V_0\left|J_l(\sqrt{2n_0h}\,)\frac{d^2J_l(\sqrt{2n_0h}\,)}{d^2n}\right|^{1/2}\ . \tag{20}$$

This expression, derived solely within quantum mechanics, becomes identical to the classical formula for the frequency of oscillations near the elliptic points on Fig. 1 ([8], formula 2.4.77).

We observe from Fig. 2 that QE levels accumulate around $E_q=0$ for each individual spectrum. Classically, $E_q=0$ corresponds to the Hamiltonian (2) being equal to zero, i.e., to the separatrix lattice (see Fig. 1), where the frequency of motion approaches zero. Therefore, the clustering of levels near $E_q=0$ is the quantum manifestation of the classical motion near the separatrix.

Hence, the main classical features of the systems described by the Hamiltonian (2) are manifested in the QE spectra of uncoupled cells. Inspection of several numerical results likes those of Fig. 2(d) have shown that the spectra calculated for the three cells can be considered essentially as a superposition of the three uncoupled cells, except near the accumulation point. The range of the combined spectrum is given by the range of the spectrum of the first cell. Each additional cell modifies the combined spectrum only within the range of each subsequent cell. Note that the range decreases monotonically (as $\sqrt{1/kr}$) and that the number of Landau states in each cell is finite. Based on these facts we conjecture (we have no rigorous mathematical proof) that the spectrum described by Eq. (18) is discrete.

We can gain an understanding about the structure of combined spectra by analyzing the nature of the QE functions A^q_n. Figure 3 shows plots of A^q_n as a function of the Landau number n. At the top of Fig. 3 we also plotted the matrix elements $V_{n,n+1}$. We note that there are states that are localized in one cell and others that are spread throughout the three cells. We shall refer to these latter ones as "partially extended." They are not expected to be fully extended since, as argued above, the spectrum is discrete. We remark that this localization or extension refers not to position space but to Landau states n. These are, in general, not equivalent. Our numerical experiments have shown that in general the localized states correspond to QE levels at the bottom and top of the combined spectrum. However, states extend over the three cells for QE levels near $E_q=0$. When we consider QE functions for uncoupled cells, we find that these are localized in the middle of the cell for QE levels at the extremes of its spectrum and extend over the whole cell for QE levels in the neighborhood of the center of its spectrum, $E_q=0$. The QE functions plotted in Figs. 3(a)–3(c) are states belonging to the upper [3(c)] and the lower [3(a),3(b)] parts of the combined spectrum. Figure 3(d) belongs to a state near $E_q=0$. The condition for states to extend throughout the number of cells under consideration is the clustering of levels around $E_q=0$. Clusterings of levels not in the vicinity of $E_q=0$ are accidental and do not yield extended QE states, because there is no overlapping at the boundaries of the cells and hence there is no significant coupling.

We now analyze the structure of the QE spectrum and QE functions for the near resonant case [see the corresponding classical picture, Fig. 1(b)]. As a representative of the near resonant case, Fig. 4 shows the combined and individual spectra for the same parameters as in Fig. 2, but with $\delta\omega=0.015$. Incidentally, the data of Fig. 4 can be used to obtain the spectrum E_q for any other values of the parameters V_0 and $\delta\omega$, as long as these vary proportionally. For example, if $V_0\rightarrow V_0/2$ and $\delta\omega\rightarrow\delta\omega/2$, then Eq. (18) gives $E_q\rightarrow E_q/2$. Now notice, in contrast to the resonant case, the lack of symmetry with respect to $E_q=0$. The spectrum (a) resembles that of the resonance case but is shifted up in energy. For the first cell, n is small, so $n\hbar\delta\omega\ll|V_{n,n+l}|$ and hence the spectrum, according to Eq. (18), is mainly determined by the off-diagonal terms $|V_{n,n+l}|$. However, spectrum (c) in Fig. 4 is nearly equidistant over most of its range and differs qualitatively from the corresponding spectrum (c) of Fig. 2. For this cell, n is large enough so that $\hbar\delta\omega n\gg|V_{n,n+1}|$. Then to zero order approximation we can neglect the off-diagonal terms $V_{n,n+1}$, and the system (18) becomes essentially unperturbed with a constant level separation $\hbar\delta\omega$, QE functions $A^q_n=\delta_{q,n}$, and Landau level functions $\Psi_{E_n}=\exp(-iE_nt/\hbar)\Psi_n(x)$ [see (14) and

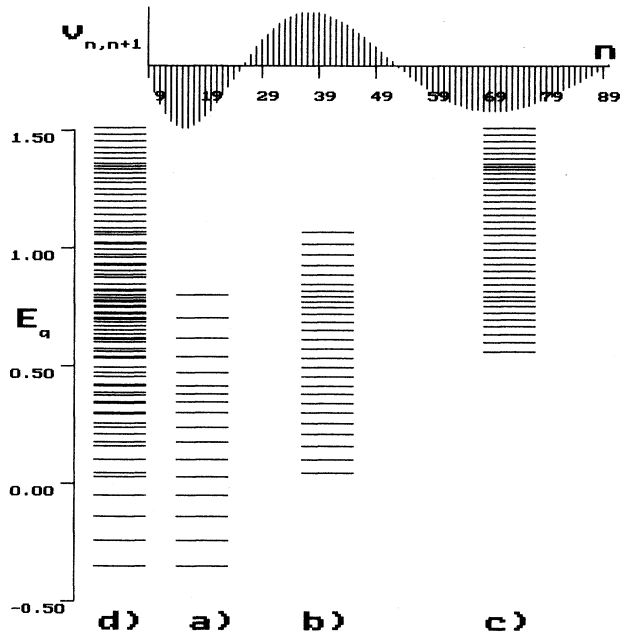

FIG. 4. QE spectrum and matrix elements for the near resonance case $\delta\omega=0.015$. The values of V_0 and h are the same as in Figs. 2 and 3.

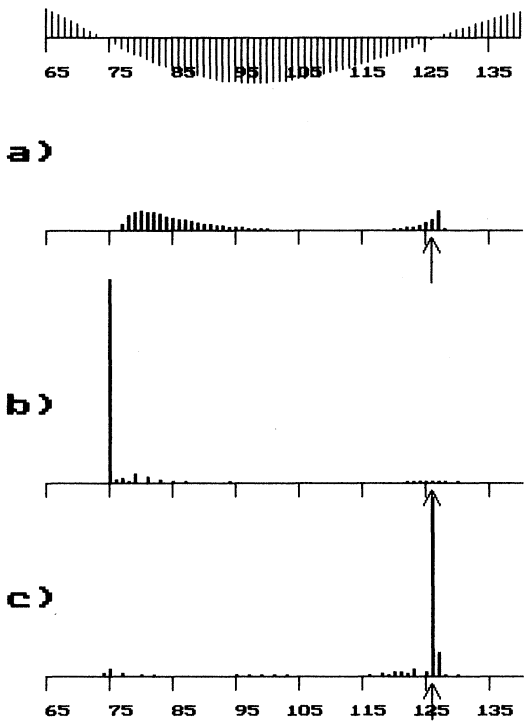

FIG. 5. Temporal evolution of the distribution $|C_n|^2$ as a function of n. Case $\delta\omega=0$. The initial Landau state, marked by an arrow, is located near the boundary of the cell. $V_0=5$, $h=0.7$.

(15)]. Note however, that there is a clustering of levels in spectrum (c) of Fig. 4. This clustering is, as in the resonant case, a manifestation of the resonance of its classical counterpart. Note that the clustering is not around $E_q=0$, which corresponds to the classical Hamiltonian (2) not being equal to zero at the separatrix.

We shall now discuss the evolution of initial states in the exact resonant case. Numerical experiments have allowed us to distinguish two types of evolution. Figure 5 shows snapshots of the evolution of the initial state, a Landau state $C_n=\delta_{n,n_0}$, located near the boundary between the fourth and fifth Hilbert cell. The initial state is marked by an arrow on the n axes. The argument of the Bessel function, $\sqrt{2n_0h}$, is close to its fourth zero. For this figure, $h=0.7$, $n_0=126$. After a few cyclotron periods (~ 3) a wave packet is formed. Figure 5(a) shows the wave packet at a later time $t=10T_c$ (T_c is the cyclotron period) traveling towards the left boundary of the cell. Then, at subsequent times, the probability distribution $|C_n|^2$ spreads throughout the whole cell and at time $t=20T_c$ it collects itself at the left boundary [see Fig. 5(b)]. At time $t=42T_c$ most of the distribution has returned to the initial position. After some periods of these types of oscillations of the distribution, a dominant peak is formed near each of boundaries of the fourth cell. As the amplitude of one grows, the other one decreases in a periodic fashion. The frequency of these oscillations corresponds to the smallest distances between QE levels. To see this behavior we can expand the δ function of the initial state in terms of the QE functions,

$$\delta_{n,n_0}=\sum_q A^q_{n_0}A^q_n \ . \tag{21}$$

So the evolution of this state will be given by

$$C_n(t)=\sum_q A^q_{n_0}A^q_n e^{-i(E_q t/\hbar)} \ . \tag{22}$$

The coefficients $A^q_{n_0}$ in the expansion (21) depend upon the position n_0 of the initial state in a given cell. When n_0 is near the boundary the main contribution in (21) comes from QE functions about the middle of the spectrum. This claim is based on the observation that only QE functions associated with QE levels near $E_q=0$ have dominant amplitudes (see Fig. 3). We also observe that all Landau levels oscillate at about the same frequency.

If the initial state is located somewhere in the middle of the cell, then it spreads much faster than in the previous case without forming any localized distribution. Figure 6 shows the distribution $|C_n|^2$ at two different times for an initial state (Landau state) located near the middle of the fourth Hilbert cell. We observe two generic features (i) the initial distribution quickly (much faster than in the previous case) spreads throughout the cell, and (ii) the frequencies of oscillations of $|C_n|^2$ are markedly different for different n. The oscillations are faster in the middle than to the neighborhood of the Hil-

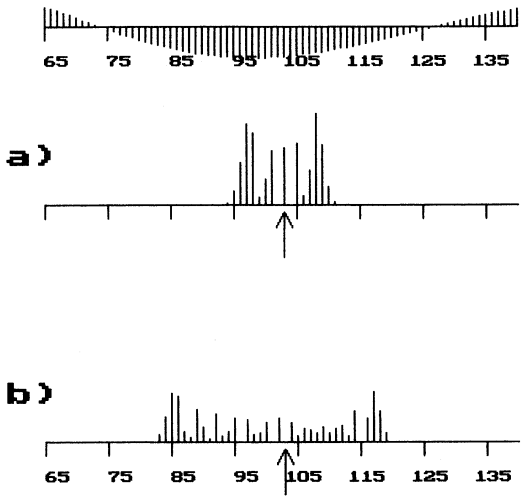

FIG. 6. Temporal evolution of the distribution $|C_n|^2$ as a function of n. Case $\delta\omega=0$. The initial Landau state, marked by an arrow, is located in the neighborhood of the center of the cell. $V_0=5$, $h=0.7$. The times are (a) $t=1T_c$ and (b) $t=3T_c$.

bert cell boundaries. We can understand this behavior with the help of the expansion (21). When the initial state δ_{n,n_0} is located at about the middle of the cell, its expansion in QE states (21) contains QE states belonging to the whole range of the spectrum (see Fig. 3). Thus there is a wide range of frequencies in the evolution of the probability distribution $|C_n|^2$.

The two distinct types of quantum motion just described make the classical-quantum corresponding of our system clearer. That is, an initial quantum state with a sharp n_0 corresponds to a definite classical value of the action I_0. For an n_0 near a Hilbert cell boundary, I_0 is close to the corresponding zero of the Bessel function $J_l(I)$, i.e., close to the separatrix. Consider a set of classical orbits, all with same initial I but with different initial θ. Each one of these will execute slow-frequency motion and with nearly the same frequency. The corresponding quantum motion is similarly characterized; namely, (i) all components $|C_n|^2$ oscillate slowly with about the same frequency, and (ii) the distribution $|C_n|^2$ shifts from one end to another of the Hilbert cell more or less periodically. In contrast, a set of classical orbits all with the same value at I_0 around the middle of the classical case but with different value of initial θ, will execute oscillatory motion with as many different frequencies as there are initially different θ's. This behavior is manifested quantum mechanically by the absence of any periodic motion and by the wide range of frequencies of oscillations of the amplitude $|C_n|^2$.

As a final remark concerning the temporal evolution of an initial quantum distribution, we note that numerical experiments show that tunneling to neighboring cells increases as the effective Planck's constant increases. This tunneling implies the transition from one cyclotron orbit to another. This interesting phenomenon deserves further investigation. The quantum-classical correspondence of our system can be extended to the near resonant case. Classically (see [8]) cyclotron resonance is suppressed in the cell where the inequality $\delta\omega \gtrsim |V_0[dJ_l(I)/dI]|$ is satisfied. This implies that the action of any trajectory is approximately constant, so quantum mechanically one expects that any initial state located in the corresponding Hilbert cell will also remain in the neighborhood of the initial position. Our numerical experiments have confirmed this conjecture.

The above considerations allows us to make some predictions about experimental observation of acoustic quantum nonlinear resonance when an ultrasound wave propagates perpendicularly to the a magnetic field in pure metals (or semimetals). Two main conditions must be satisfied for the observation of this phenomenon: (i) the electron relaxation time τ must be larger than the typical time of spreading of initial Landau state driven by the monochromatic acoustic wave. A rough estimate gives $\tau \gg \tilde{\omega}^{-1}$; (ii) the argument of the Bessel function kr must be large enough (i.e., larger than the first zero of the Bessel function of order 1) to form one or more Hilbert cells.

Both conditions can be satisfied by the following experimental parameters: Sound frequencies of the order of 10 GHz (see, e.g., [15]), $\tau \gtrsim 10^{-9}$ sec, and sound intensity of the order at 10 W/cm^2. When these conditions are met one can observe some interesting effects, such as the attenuation of de Hass–van Alfen oscillations, Shubnikov–de Hass and quantum-Hall-effect oscillations in semiconductor heterostructures. All of these phenomena are connected with the change in the number of the filled Landau levels (with a variation of the applied magnetic field). In accordance with the results of this paper, when nonlinear cyclotron resonance takes place the sharp boundary between filled and unfilled states disappears. In other words, the electron wave function in the presence of the sound wave becomes a superposition of the several Landau states, belonging to one cell. Spreading of the wave function causes all of the oscillation phenomena to wash out. We remark that the absence of the sharp boundary between the filled and unfilled Landau states is the reason for the decrease of the sound damping coefficient under the condition of nonlinear acoustic cyclotron resonance, in comparison with the linear regime.

This work was partially supported by CONACYT, Mexico, Project No. 2065E932, International Soros Science Foundation Grant No. H3000, and by a Grant of the High School Committee of Russia. V.Y.D. thanks the Instituto de Fisica at Puebla for their hospitality, and G.L.-A wishes to thank the Welch Foundation for partial support of this work by Grant No. 1051.

[1] G. P. Berman and A. R. Kolovsky, Physica **8D**, 117 (1983); Phys. Lett. A **95**, 15 (1983); G. P. Berman and G. M. Zaslavskii, Phys. Lett. A **61**, 295 (1977).
[2] L. E. Reichl and W. A. Lin, Phys. Rev. A **33**, 3598 (1986).
[3] M. Toda and K. Ikeda, J. Phys. A **20**, 3833 (1987).
[4] T. Geisel, G. Radons, and J. Rubner, Phys. Rev. Lett. **57**, 2883 (1986).
[5] S. Dyrting, G. J. Milburn, and C. A. Holmes, Phys. Rev E **48**, 969 (1993).
[6] C. F. F. Karney and A. Bers, Phys. Rev. Lett. **39**, 550 (1977).
[7] A. Fukuyama and H. Matota, Phys. Rev. Lett. **38**, 701 (1977).
[8] A. J. Lichtenberg and M. A. Lieberman, *Regular and Stochastic Motion* (Springer, New York, 1983), Chap. 2.
[9] V. A. Burdov and V. Ya. Demihovski, Zh. Eksp. Teor. Fiz. **70**, 194 (1990) [Sov. Phys. JETP **70**, 194 (1990)].
[10] A. A. Chernikov, R. Z. Sagdeev, D. A. Usikov, and G. M. Zaslavskii, Comput. Math. Appl. **17**, 17 (1989); A. A. Chernikov, R. Z. Sagdeev, D. A. Usikov, M. Yu. Zakharov, and G. M. Zaslavskii, Nature **326**, 559 (1987); G. M. Zaslavskii, D. A. Usikov, and A. A. Chernikov, *Weak Chaos and Quasiregular Structures* (Nauka, Moscow, 1990) (in Russian).
[11] G. P. Berman, V. Uy. Rubaev, and G. M. Zaslavskii, Nonlinearity **4**, 543 (1991); D. Shepeliansky and C. Sire, Europhys. Lett. **20**, 95 (1992); A. A. Chernikov, R. Z. Sagdeev, D. A. Usikov, and G. M. Zaslavskii, Comput. Math. Appl. **17**, 17 (1989); G. M. Zaslavskii, D. A. Usikov, and A. A. Chernikov, *Weak Chaos and Quasiregular Structures* (Nauka, Moscow, 1990) (in Russian).
[12] I. S. Gradstein and I. M. Ridjic, *Tables of Integrals, Sums, Sets, and Products* (Nauka, Moscow, 1963) (in Russian).
[13] L. E. Reichl, *The Transition to Chaos* (Springer-Verlag, New York, 1992).
[14] G. M. Zaslavskii, *Chaos in Dynamic Systems* (Harwood Academic, Chur, Switzerland, 1985).
[15] R. L. Willet, R. R. Ruel, K. W. West, and L. N. Pfeiffer, Phys. Rev. Lett. **71**, 3846 (1993).